Environmental Science & Technology

pubs.acs.org/est

Article

Biogenic Palladium Improved Perchlorate Reduction during Nitrate Co-Reduction by Diverting Electron Flow in a Hydrogenotrophic Biofilm

Jingzhou Zhou, Lin Yang, Xiaodi Li, Ben Dai, Junxia He, Chengyang Wu, Si Pang, Siqing Xia,* and Bruce E. Rittmann

Cite This: https://doi.org/10.1021/acs.est.4c01496

Read Online

ACCESS | Metrics & More | Article Recommendations | Supporting Information

ABSTRACT: Microbial reduction of perchlorate (ClO_4^-) is emerging as a cost-effective strategy for groundwater remediation. However, the effectiveness of perchlorate reduction can be suppressed by the common co-contamination of nitrate (NO_3^-). We propose a means to overcome the limitation of ClO_4^- reduction: depositing palladium nanoparticles (Pd^0NPs) within the matrix of a hydrogenotrophic biofilm. Two H_2-based membrane biofilm reactors (MBfRs) were operated in parallel in long-term continuous and batch modes: one system had only a biofilm (bio-MBfR), while the other incorporated biogenic Pd^0NPs in the biofilm matrix (bioPd-MBfR). For long-term co-reduction, bioPd-MBfR had a distinct advantage of oxyanion reduction fluxes, and it particularly alleviated the competitive advantage of NO_3^- reduction over ClO_4^- reduction. Batch tests also demonstrated that bioPd-MBfR gave more rapid reduction rates for ClO_4^- and ClO_3^- compared to those of bio-MBfR. Both biofilm communities were dominated by bacteria known to be perchlorate and nitrate reducers. Functional-gene abundances reflecting the intracellular electron flow from H_2 to NADH to the reductases were supplanted by extracellular electron flow with the addition of Pd^0NPs.

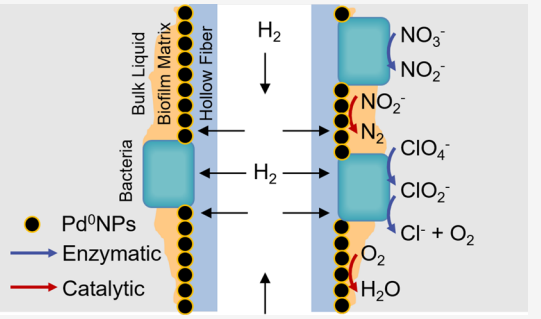

KEYWORDS: *palladium nanoparticles, Pd-catalyzed reduction, intracellular electron transfer, perchlorate reduction*

INTRODUCTION

Worldwide, groundwater has been contaminated with perchlorate (ClO_4^-) due to its widespread use in solid rocket fuels, lubricating oils, pyrotechnics, and munitions.[1,2] ClO_4^- contamination in groundwater generally is <100 μg/L although it can reach or exceed 20 mg/L near ordnance factories.[3] Perchlorate poses serious health threats to human beings by interfering with the uptake of iodide and subsequently inhibiting the thyroid's hormone production.[4] The World Health Organization (WHO) set a limit for ClO_4^- of 0.07 mg/L in its Guidelines for Drinking Water Quality (GDWQ).[5]

Adsorption, ion exchange, and membrane filtration have been employed to remove ClO_4^-, but they are energy-intensive and costly; they generate a highly contaminated brine.[6] In contrast, bioreduction of ClO_4^- is a lower-energy and lower-cost strategy that does not generate a brine.[7] The key to bioreduction is supplying a readily biodegradable electron-donor substrate. Compared to traditional organic electron donors — such as acetate, methanol, and lactate — hydrogen gas (H_2) and short-chain gaseous alkanes (e.g., methane, ethane) are promising electron donors for perchlorate bioremediation due to their advantages: relatively low cost, minimal electron-donor residual, and widespread availability. Delivering the gaseous donor via nonporous membranes that accumulate a biofilm has been demonstrated for ClO_4^- reduction.[3,8,9] An important factor is that nitrate (NO_3^-) is a common cocontaminant that often is present at a much higher concentration.[10] In this situation, perchlorate reduction can be suppressed by competition from NO_3^-, even when the electron donor is available in excess.[11]

In dissimilatory ClO_4^- bioreduction, ClO_4^- is reduced in a three-step process. Perchlorate reductase (PcrAB) catalyzes the first two steps: reduction of ClO_4^- to chlorate (ClO_3^-) and subsequent reduction of ClO_3^- to chlorite (ClO_2^-), with NADH (the reduced form of nicotinamide adenine dinucleotide) as the intracellular electron donor in both steps. The bacteria use a chlorite dismutase (Cld) to catalyze ClO_2^- cleavage into innocuous chloride ion (Cl^-) and molecular O_2 at a high rate ($k = 2.0 \times 10^5$ s^{-1}).[12,13] The O_2 is reduced in respiration by complex IV.[14] Intracellular NADH is generated by hydrogenase-catalyzed oxidation of H_2 in hydrogenotrophic

Received: February 12, 2024
Revised: March 20, 2024
Accepted: April 15, 2024

biofilm.[15] Respiration involves the transfer of electrons from NADH to several reductases that catalyze reductions of ClO_4^-, ClO_3^-, O_2, NO_3^-, and NO_2^-. This means that all respiratory reductions compete for common NADH.

Here, we evaluate a strategy to eliminate the competition from NO_3^-: depositing palladium nanoparticles (Pd^0NPs) within the matrix of a hydrogenotrophic biofilm. Pd^0NPs immobilized in the biofilm matrix adsorb H_2 and cleave it to form activated H atoms (i.e., H*) to form [Pd−H*], which can reduce a number of drinking-water contaminants, particularly NO_2^-.[16−18] Pd^0NP-catalyzed hydrogenation can lower intracellular competition for NADH and accelerate respiration, which must occur intracellularly. Previous work documented an acceleration of the NO_3^- reduction due to synchronous enzymatic and catalytic reductions: NO_3^- reduction to NO_2^- was entirely accomplished by bacteria, while NO_2^- reduction to N_2 was primarily catalyzed by Pd^0NPs.[19−21] When ClO_4^- and NO_3^- co-reductions occur, diversion of electron flow away from intracellular NADH consumption for NO_2^- reduction to extracellular Pd^0NP-catalyzed reduction may enhance ClO_4^- reduction during NO_3^- co-reduction by lowering the intracellular demand for NADH.

This study assessed the impact of Pd^0NP-catalyzed hydrogenation on intracellular ClO_4^- reduction within the context of NO_3^- co-reduction in a hydrogenotrophic biofilm. This was achieved by comparing the reduction performances of two parallel H_2-MBfRs operated in long-term continuous and batch modes. One system had only a biofilm, while the other incorporated biogenic Pd^0NPs in the biofilm matrix. Differences in the structure of the biofilm microbial community and functional gene abundance were analyzed.

MATERIALS AND METHODS

MBfR Configuration. Operated in parallel were two identical MBfRs, shown in Figure S1 and similar to our previous studies.[22,23] Each MBfR comprised a main column containing a 32-fiber bundle and a sampling column containing a 20-fiber coupon bundle for biofilm sampling. The fibers were nonporous polypropylene hollow fibers (Teijin, Japan), which supplied bubble-free H_2 on-demand H_2 to the biofilm attached to the exterior surface. A peristaltic pump created completely mixed conditions in each MBfR by setting a recirculation rate of 100 mL/min. The temperature was maintained at 25 ± 1 °C. Details of physical parameters are summarized in Table S1.

Biofilm Inoculation and Biogenic Palladium Deposition. During biofilm inoculation and Pd^0 deposition, H_2 was supplied to the MBfRs at a rate of 1.5 atm (absolute pressure). The inoculum was collected from an anaerobic-anoxic-oxic (AAO) reactor in the laboratory.[24] The inoculum was divided into two equal portions, and one portion was injected into each of the parallel MBfRs. The inoculum was allowed to attach on the exterior surface of the fibers to initiate the biofilm for 48 h. Then, one of the MBfRs was drained and refed with a 100 mL medium containing Pd(II) (2 mM Na_2PdCl_4) in a 5-mM phosphate buffer at pH 8 to create a bioPd-MBfR.[21,25] The Pd(II) concentration was analyzed by inductively coupled plasma−mass spectrometry (ICP-MS) (ICPMS 7700, Agilent, USA). More than 99% of the added Pd(II) was reduced to biogenic nanoparticle palladium (Pd^0NPs) on the biofilm over 24 h. The total accumulation was 21 mg of Pd^0NPs, giving a Pd^0 loading of 3.9 g of Pd^0NPs/m^2 for the bioPd-MBfR. The MBfR without Pd^0NPs is called the bio-MBfR.

We also created a Pd-containing membrane-film reactor (Pd-MfR) without biofilm for batch tests using the same Pd^0-deposition method as for the bioPd-MBfR. It also had a Pd^0 surface loading of 3.9 g Pd^0NPs/m^2.

Continuous Operation of the bio- and bioPd-MBfRs. The two MBfRs were operated in parallel by using exactly the same operating conditions. The feeding medium during the entire operation contained 0.170 g KH_2PO_4, 0.100 g Na_2HPO_4, 0.100 g $NaHCO_3$, 1 mL trace element A solution, and 1 mL trace element B solution in 1 L of deionized water. The compositions of the trace-element stock solution are summarized in Section S2. Before being fed to the MBfRs, the medium was stored in the influent tank and deoxygenated by sparging with 99.99% N_2 gas for 20 min. The HRT of each MBfR was maintained at 4 h over 100 days of continuous operation. Changes in the ClO_4^- and NO_3^-−N concentration (provided as $KClO_4$ and $NaNO_3$) and the supplied H_2 (99.99%) pressure are summarized in Table 1. Each stage was operated until the effluent concentration of ClO_4^- and NO_3^-−N had ≤5% variation for at least 3 HRTs.

Table 1. Operating Conditions for Each Stage

stage	NO_3^-−N/mg L^{-1}	ClO_4^-/mg L^{-1}	H_2/atm	duration/days
S0	10	2	1.50	23
S1	10	4	1.50	15
S2	15	4	1.50	15
S3A	15	4	1.68	22
S3B	15	4	2.02	14
S4	10	2	1.50	14

Chemical Analyses. Effluent samples were filtered through a 0.22-μm membrane filter (25 mm PES, Titan, China) immediately after daily collection using a 10 mL syringe. The concentrations of ClO_4^-, ClO_3^-, ClO_2^-, NO_3^-−N, and NO_2^-−N were assayed by an ion chromatograph (Dionex Aquion, USA) with an AS20 column and AG20 precolumn, an eluent concentration of 10 mM KOH, and a 1 mL/min flow rate. Considering that N_2O and NO did not accumulate during denitrification under circumneutral pH conditions[26] and in the Pd-catalyzed NO_3^- reduction process,[19] N_2O and NO were not examined as intermediates in this study. The concentration of NH_4^+−N was determined by the standard methods.[27] No accumulation of NO_2^-−N, NH_4^+−N, ClO_3^-, or ClO_2^- was detected in the effluent of the MBfRs during continuous operation. The pH of the medium was measured with a pH meter (HQ1110, HACH, USA).

Flux Calculations. The theoretical maximum H_2 flux (e^- eq/m^2 d) was calculated by[28]

$$J_{H_2,max} = \frac{K_m}{z_m}(P_0 - P_{m-lf})k_1\frac{d_m - z_m}{d_m} \quad (1)$$

where K_m is the H_2 permeability (m^3 H_2 @ standard temperature and pressure m membrane thickness/m^2 hollow fiber surface area d bar), z_m is the membrane thickness (m), P_0 is the H_2 pressure in the hollow-fiber lumen (bar), P_{m-lf} is the H_2 pressure in the interface of membrane and liquid film and was set to 0 to give the maximum flux, k_1 is the coefficient that converts H_2 from volume to mass (1 g/0.0112 m^3 @ standard temperature and pressure), and d_m is the hollow fibers' outer diameter (m).

https://doi.org/10.1021/acs.est.4c01496
Environ. Sci. Technol. XXXX, XXX, XXX−XXX

The NO_3^-−N and ClO_4^- reduction fluxes expressed in electron equivalents (eq e^-/m^2 d) were computed by

$$J_{NO_3^-N} = \frac{5}{14} \times \frac{Q(S_0 - S)}{A} \quad (2)$$

$$J_{ClO_4^-} = \frac{8}{99.5} \times \frac{Q(S_0 - S)}{A} \quad (3)$$

where S_0 and S are the influent and effluent oxyanion concentration (g/L), Q is the influent flow rate to the MBfRs (L/d), A is the membrane surface area (m^2), 5 is the number of e^- eq to reduce NO_3^- to N_2, 8 is the number of e^- eq to reduce ClO_4^- to Cl^- and H_2O, 14 is the molecular weight of N, and 99.5 is the molecular weight of ClO_4^-.

Batch Tests in the MBfRs. We carried out parallel batch tests using media containing ClO_4^- or ClO_3^- alone in bio-MBfR, bioPd-MBfR, and Pd-MBfR. Batch tests are conducted with 1.50 atm of H_2 and between continuous-flow stages S3B and S4. Liquid samples were taken at 0, 10, 20, 30, 60, 90, 120, 180, 240, and 300 min. During the interval of the batch tests, the MBfRs were fed with a medium containing low concentrations of ClO_4^- and NO_3^-, similar to that of S4. In addition, a set of batch tests were conducted in the same manner but without H_2 supplied.

Biofilm Morphology and Solid-State Characterization. At the end of S4, ∼3 cm-long coupon fibers of bioPd-MBfR were cut off for transmission electron microscopy (TEM, JEOL JEM-F200, Japan) equipped with energy dispersive X-ray spectroscopy (EDS, Bruker Quad 5040, Germany). Both main-column fibers of bio-MBfR and bioPd-MBfR were desiccated in a freeze-dryer (FD1A-50, BILON, China). The structure of the desiccated biofilm was analyzed by using X-ray diffraction (XRD) with a Cu−Kα radiation source (40 kV, 40 mA) and an X-ray diffractometer (Rigaku Ultima IV, Japan). X-ray photoelectron spectroscopy (XPS) was applied to analyze the valence state of Pd in desiccated biofilm through a Thermo Scientific K-Alpha (ThermoFisher, USA).

Biofilm Community and Function Analyses. Biofilm samples were collected at the end of samples S2, S3B, and S4. We cut off 18 cm-long sections from a coupon fiber from bio-MBfR and bioPd-MBfR. The open end of the remaining fiber was tied with 2 knots to avoid H_2 leakage. Genomic DNA was extracted with a DNeasy PowerBiofilm Kit (QIAGEN GmbH, Germany) according to the manufacturer's specifications. DNA was quantified by Picogreen on a Quantus fluorometer (Promega, USA) and absorbance (Nanodrop 2000, USA). DNA contamination was detected by 1% agarose gel electrophoresis. The metagenomic sequencing and analysis processes are described in Section S4.

Microbial Community taxonomic annotations were conducted against the NCBI-nr database using representative sequences of the nonredundant gene catalog. Functional annotation was conducted against the Kyoto Encyclopedia of Genes and Genomes (KEGG) database and Clusters of Orthologous Groups of proteins (COG) databases using the DIAMOND alignment algorithm with an e-value cutoff of $1 \times e^{-5}$. The gene abundance was normalized by Reads Per Kilobase Per Million mapped (RPKM).[29]

$$\mathrm{RPKM}_i = \frac{(R_i/L_i) \times 10^6}{L_i \times \sum_1^n (R_j)} \quad (4)$$

in which R_i represents the number of reads of gene$_i$ (KB) in a certain sample; L_i represents the nucleotide length of Gene$_i$; and $\sum_1^n(R_j)$ represents the sum of reads corresponding to all genes in the sample (KB). The gene set and calculation results are listed in Table S2. All data from DNA samples' sequencing were deposited at the National Center for Biotechnology Information (NCBI)/Sequence Read Archive (SRA) under project PRJNA1067193.

RESULTS AND DISCUSSION

Biogenic Pd^0NPs Associated with the Biofilms Matrix. Figure 1 illustrates the retention and dispersion of biogenic

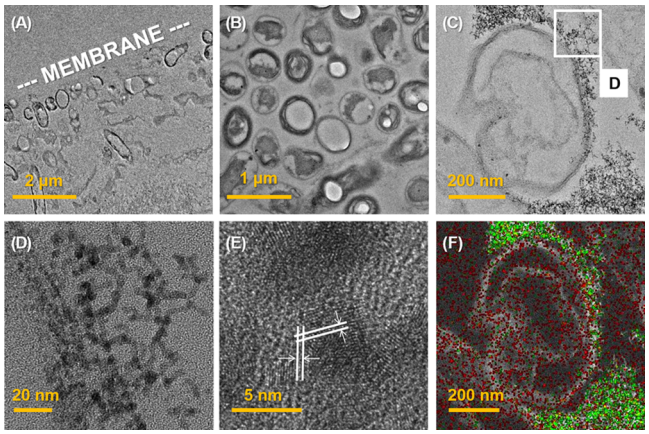

Figure 1. BioPd-MBfR fibers TEM imaging observed at 2k × (A), 6k × (B), 25k × (C), 200k × (D), 1000k × (E), and Pd (green) + O (red)-element EDS mapping (F) of (C).

PdNPs in the biofilm of bioPd-MBfR. Figure 1A shows the biofilm matrix associated with the membrane fiber. Figure 1B,C,F reveals that the majority of PdNPs were well-dispersed around a bacterial cell within the biofilm matrix. The greater magnification in Figure 1D shows that the PdNPs had a diameter of 3.4 ± 0.7 nm based on 50 NPs. The lattice fringes of the NPs (Figure 1E) confirm the dominant (1 1 1) planes of Pd^0, and Figure S2A points out four distinct diffraction peaks of the bioPd biofilm that align with the Pd^0's feature-dominant facets: 40.1° (1 1 1), 46.7° (2 0 0), 68.1° (2 2 0), and 82.1° (3 1 1). Figure S2B shows that Pd^0 was the predominant valence state for the Pd precipitates.

Co-Reduction of ClO_4^- and NO_3^- in Parallel MBfRs. Figure 2A summarizes the influent concentration of ClO_4^- (inf. ClO_4^-), effluent ClO_4^- concentration of bioPd-MBfR (eff. bioPd ClO_4^-), and the effluent of bio-MBfR (eff. bio ClO_4^-). Figure 2B summarizes the concentrations of NO_3^-−N, and Figure S3 presents the e^--eq fluxes.

Quicker Start-Up of ClO_4^--Reduction in bioPd-MBfR. In S0, 2 mg/L ClO_4^- and 10 mg/L NO_3^-−N were fed to bio- and bioPd-MBfRs, and both realized stable ClO_4^- and NO_3^-−N reductions. However, bioPd-MBfR achieved an effluent ClO_4^- concentration <0.2 mg/L by Day 2, while bio-MBfR required 12 days to reach 0.2 mg/L. The effluent NO_3^-−N of both MBfRs stabilized at 0.6 ± 0.1 mg/L during the 23 days of S0.

Better Performance of bioPd with Higher Loading. When the ClO_4^- loading was doubled in S1, the average ClO_4^- effluent concentration in bioPd-MBfR increased to 0.6 ± 0.1 mg/L, compared to an increase to 1.2 ± 0.03 mg/L for bio-MBfR. The average effluent concentration of NO_3^-−N decreased to 0.1 ± 0.1 mg/L in bioPd-MBfR, but it increased

https://doi.org/10.1021/acs.est.4c01496
Environ. Sci. Technol. XXXX, XXX, XXX−XXX

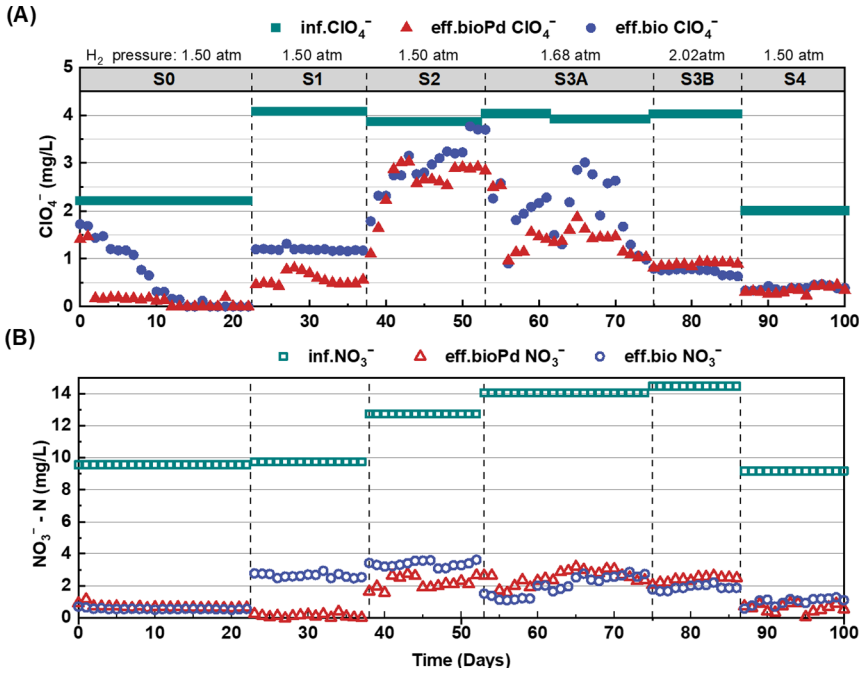

Figure 2. Reduction performance for ClO_4^- (A) and NO_3^- (B) in bioPd-MBfR and bio-MBfR. The corresponding e^--eq fluxes are in Figure S3.

to 2.6 ± 0.1 mg/L in bio-MBfR. As a result, the total oxyanion-reduction flux (Figure S3A) of bioPd-MBfR increased, but it decreased in bio-MBfR. The increased ClO_4^- loading led to higher reduction fluxes of ClO_4^- and NO_3^-−N in bioPd-MBfR (Figure S3B,C), but the NO_3^-−N reduction flux declined in bio-MBfR.

When the influent concentration of NO_3^-−N was increased from 10 to 15 mg/L in S2, the e^--eq delivery flux needed for total-oxyanion reduction exceeded the H_2 supply, and this strongly suppressed ClO_4^--reduction (Figure S3). Even though both MBfRs had higher effluent ClO_4^- than that in S1 (Figure 2A), bioPd-MBfR performed better than bio-MBfR for ClO_4^- and NO_3^-−N reductions. For example, the effluent concentration of NO_3^-−N was 2.6 ± 0.4 mg/L for bioPd-MBfR versus 3.4 ± 0.2 mg/L for bio-MBfR (Figure 2B).

Lower Selectivity toward Nitrate Reduction for bioPd-MBfR. Going from S2 to S3A, the reduction flux of oxyanions increased with the increasing supply of H_2 gas (the H_2-delivery capacity increased from 362 eq e^- /m^2 d to 407 eq e^- /m^2 d), which was closer to the average H_2 delivery flux for full oxyanion reduction (436 ± 7 eq e^- /m^2 d). The distribution of electron flux showed an increase in the proportion for ClO_4^- from 2.3 to 4.2% in bioPd-MBfR which was higher than the 1.9% to 3.0% observed in bio-MBfR. Additionally, the reduction flux of ClO_4^- in bioPd-MBfR increased more than bio-MBfR: from 8 ± 3 eq e^- /m^2 d to 15 ± 3 eq e^- /m^2 d for bioPd-MBfR versus from 6 ± 3 eq e^- /m^2 d to 12 ± 4 eq e^- /m^2 d for bio-MBfR. Comparing S3A with S2, bioPd-MBfR favored ClO_4^- reduction as the H_2-delivery capacity increased to close to ∼90% of the stoichiometric demand for full oxyanion reduction.

Pivotal Role of the Biofilm in bioPd. In S3B, the maximum H_2 flux was elevated to 490 eq e^- /m^2 d, which exceeded the H_2-delivery flux needed for total-oxyanion reduction. The ClO_4^--reduction flux in the bioPd-MBfR stabilized at 20 ± 0.2 eq e^- /m^2 d (80% of the ClO_4^- load flux), while the ClO_4^- reduction flux in the bio-MBfR was 21 ± 0.3 eq e^- /m^2 d (84% of the ClO_4^- load flux). Although the increase of H_2 supply led to a higher active H* coverage on Pd^0NPs surface,[30] the stability of ClO_4^- reduction in bioPd-MBfR implies that the higher active H* coverage did not contribute to an increase in ClO_4^- reduction because ClO_4^- is not catalytically reduced by Pd^0NPs.[31]

Figure 3 summarizes the results of the batch tests. In the presence of H_2, more rapid reductions of ClO_4^- and ClO_3^- were observed with bioPd-MBfR compared to bio-MBfR (Figures 3A,B). Furthermore, no ClO_4^- reduction occurred in the absence of H_2 (Figure 3D). Pd-MfR showed no significant

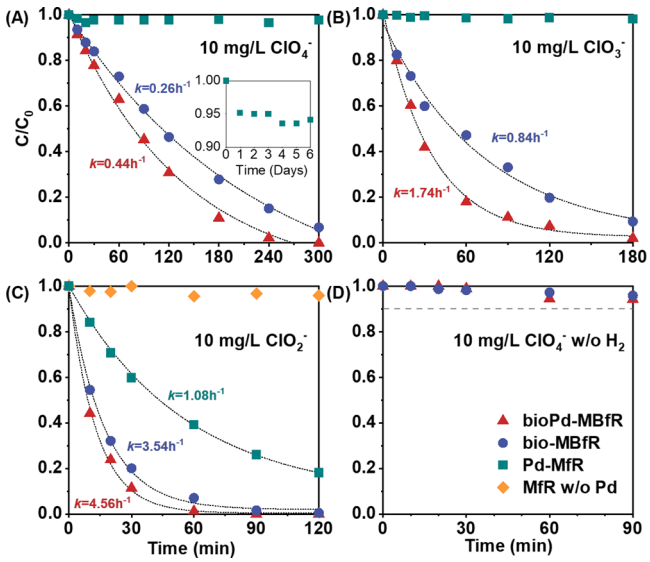

Figure 3. Batch kinetic profiles of Cl species as the sole terminal electron acceptor (no NO_3^- present). Ten mg/L initial ClO_4^- (A), 10 mg/L initial ClO_3^- (B), 10 mg/L initial ClO_2^- (C), and 10 mg/L initial ClO_4^- without H_2 supplied (D) in parallel MBfRs. The dotted lines are first-order fits of the experimental data, and all $R^2 \geq 0.987$.

https://doi.org/10.1021/acs.est.4c01496
Environ. Sci. Technol. XXXX, XXX, XXX−XXX

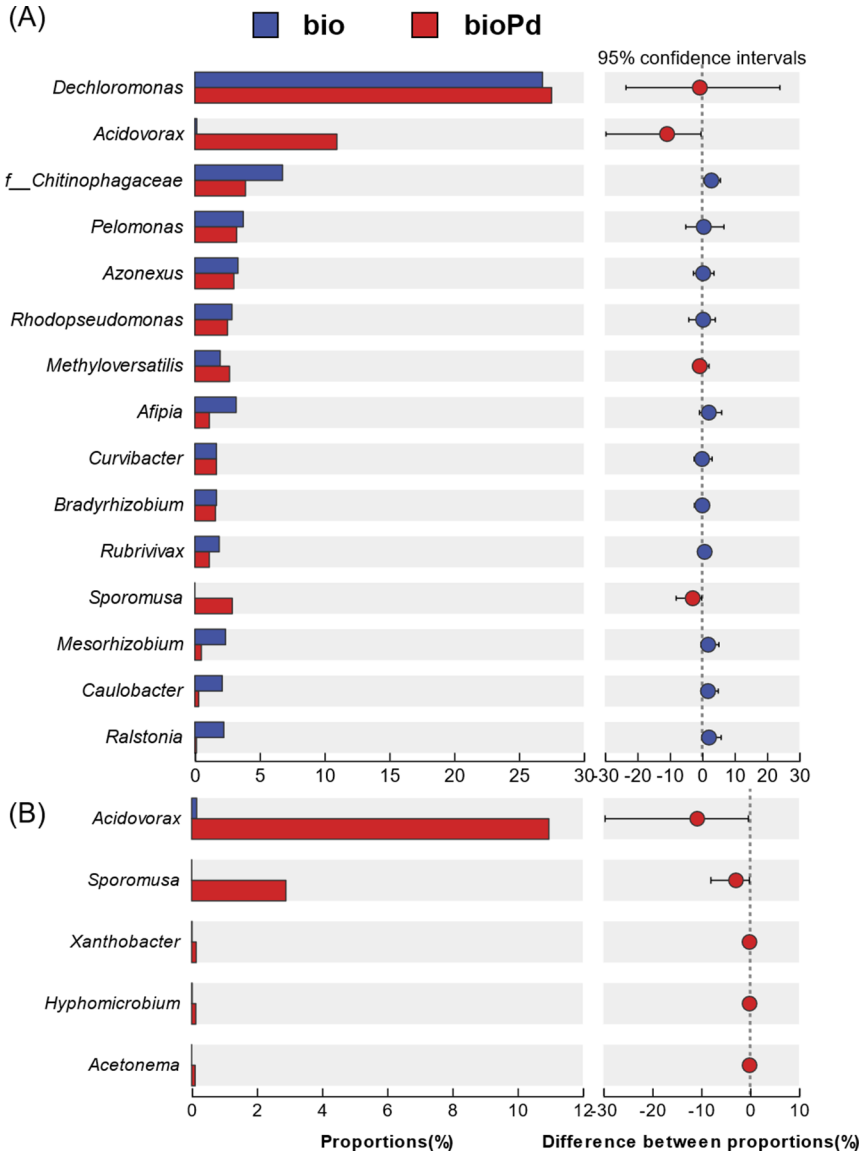

Figure 4. Average relative abundance of bacterial genera during stages in bioPd-MBfR and bio-MBfR. (A) Dominate genera in abundance (relative abundance >1% in both groups). (B) Genera with significant differences in abundance ($p < 0.1$).

reductions of ClO_4^- or ClO_3^-, consistent with previous results.[31] These results for ClO_4^- reinforce that the improved reduction efficiency observed for ClO_4^- in bioPd-MBfR was from the microbiological activity.

ClO_2^- removal was observed in bio-MBfR, bioPd-MBfR, and Pd-MfR (Figure 3C). The removal rate was slightly greater for bioPd-MBfR than for bio-MBfR, which may have been the result of reduction of ClO_2^- (to Cl^-) by Pd^0NPs occurring in parallel to bacterial dismutation of ClO_2^- to O_2 and Cl^-. Pd^0NP-catalyzed reduction also may have reduced competition for NADH with downstream O_2 reduction for respiration.

In S4, the low load led to an effluent concentration of 0.3 ± 0.07 mg/L ClO_4^- for bioPd-MBfR compared to 0.4 ± 0.04 mg/L ClO_4^- for bio-MBfR, and 0.6 ± 0.3 mg/L NO_3^- for bioPd-MBfR compared to 1.0 ± 0.2 mg/L NO_3^- for bio-MBfR on average. These results indicate a better performance of bioPd-MBfR after the shock of batch tests.

Biofilm Community Structure. *ClO_4^- and NO_3^- Shaped the Community in Both Biofilms.* Figure 4A illustrates the average relative abundances of the dominant bacteria in MBfRs. *Dechloromonas*, the dominant genera in bio-MBfR (27%) and bioPd-MBfR (28%), is a perchlorate-reducing bacterium (PRB) and denitrifying bacterium (DB).[32,33] *Acidovorax* occupied 11% in the bioPd-MBfR, but only 0.2% in bio-MBfR. Notably, *Acidovorax* is a mixotrophic PRB and DB that also can utilize acetate as its electron, which means the ability to utilize acetate may benefit its competitive advantage.[34,35] Other important genera in bio-MBfR and bioPd-MBfR were f_*Chitinophagaceae*,[36,37] *Pelomonas*,[6] *Azonexus*,[38] *Methyloversatilis*,[9] *Curvibacter*,[39] and *Mesorhizobium*,[39] which also have been identified as PRB and DB. *Afipia*, also identified as DB, but not a PRB, appeared more in bio-MBfR.[40] The dominant genera in MBfRs were mostly identified as both PRB and DB, indicating a competitive advantage of microorganisms capable of utilizing ClO_4^- and NO_3^- simultaneously in the biofilm. Figure 4B summarizes the genera with significant differences in abundances between bio-MBfR and bioPd-MBfR ($p < 0.1$). *Sporomusa* occupied 2.9% in bioPd-MBfR, compared to a minimal 0.002% in bio-MBfR. *Sporomusa*, identified as a PRB and acetogenic bacterium,

https://doi.org/10.1021/acs.est.4c01496
Environ. Sci. Technol. XXXX, XXX, XXX−XXX

exhibited a notable presence in bioPd-MBfR.[41] *Xanthobacter* and *Hyphomicrobium,* which appeared in consortia of bacteria carrying out ClO_4^- and NO_3^- reduction, also appeared more in bioPd-MBfR.[6,42] *Acetonema*, an H_2-oxidizing acetogenic bacterium, also had higher abundance in bioPd-MBfR.[43] Enrichment of acetogenic bacteria and acetate-utilizing bacteria suggests the potential for cooperative interactions in bioPd-MBfR. The variable functions of the bacteria more prevalent in bioPd-MBfR imply the presence of cooperative interactions within the biofilm matrix and underscore the significant impact of Pd^0NPs on shaping the biofilm community and its bacterial interactions.

Effect of Pd^0NP on Functional Genes. The abundances of functional genes related to NO_3^- and ClO_4^- reductions are evaluated by the odds ratios of average functional gene abundance in bioPd-MBfR compared to bio-MBfR in Figure 5.

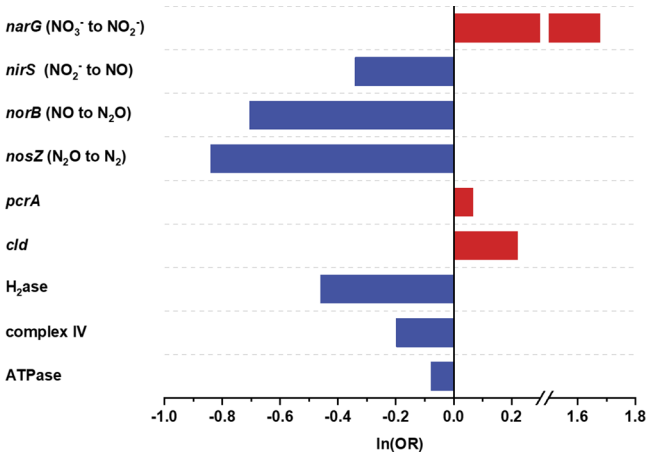

Figure 5. Odds ratios of average functional-gene abundance in bioPd-MBfR compared to those in bio-MBfR. A red bar indicates a higher abundance in bioPd-MBfR, and a blue bar indicates a higher abundance in bio-MBfR.

The dominant trend in Figure 5 is that the three genes for reducing NO_2^- to N_2 (*nirS*, *norB*, and *nosZ*) were greatly diminished in the bioPd-MBfR's biofilm, while the gene for NO_3^- reduction to NO_2^- (*narG*) was greatly increased. This reflects that reductions beginning with NO_2^- were carried out by extracellular Pd^0NP catalysis, which means that the intracellular electron flow from H_2 to NADH to the reductases was supplanted by the extracellular electron flow. Reinforcing this understanding is that the abundances of hydrogenase (H_2ase) for bacterial oxidation of H_2, Complex IV for bacterial reduction of O_2, and ATPase also were less in the biofilm of bioPd-MBfR as the bacteria has less intracellular electron flow.[14,44] The genes relating to perchlorate reduction (*pcrA* and *cld*) increased in the biofilm of bioPd-MBfR, and this is consistent with a faster ClO_4^- reduction in bioPd-MBfR (Figure 3).

Figure 6 is a schematic summarizing how the presence of Pd^0NPs in the biofilm of bioPd-MBfR shifts some electron flow from intracellular to extracellular. NO_3^- to NO_2^-, ClO_4^- reduction to ClO_3^-, subsequently to ClO_2^-, and finally to Cl^- and O_2 are catalyzed by relevant reductases. Meanwhile, NO_2^- reduction to N_2 and O_2 reduction to H_2O are catalyzed by extracellular Pd^0NPs, lowering intracellular competition for NADH and leading to faster bacterial reductions of ClO_4^-, ClO_3^-, and ClO_2^-. Hence, genera with both ClO_4^- and NO_3^-

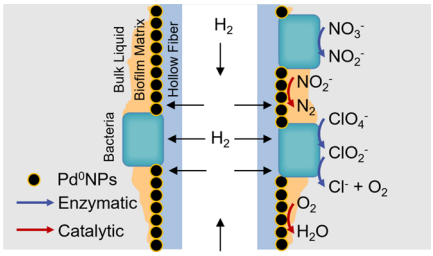

Figure 6. Schematic representation of the extracellular electron transfer in bioPd-MBfR.

reduction capabilities are more likely to gain an advantage in competition compared to denitrifiers, thereby enhancing the ClO_4^- reduction in the biofilm of bioPd-MBfR.

ENVIRONMENTAL IMPLICATIONS

This work explains how the presence of Pd^0NPs in a hydrogenotrophic biofilm shifted electron flow from intracellular via NADH to extracellular by Pd^0NPs-catalyzed hydrogenation. Performance results, reinforced by changes in the abundances of functional genes, revealed that adding Pd^0NPs to the biofilm significantly improved ClO_4^- reduction in the presence of NO_3^- by having the reductions of NO_2^- to N_2 and O_2 to H_2O occur outside the bacteria, which allowed more intracellular NADH to be used for ClO_4^- reduction. The results document that utilizing the bioPd-MBfR platform enables faster and more reliable co-reduction of ClO_4^-, and it likely will be similarly applicable to co-reduction of a broad spectrum of oxidized contaminants, such as bromate (BrO_3^-), iodate (IO_3^-), trichloroethene, trichloroethane, and per- and poly-fluorinated alkanoic substances (PFAS).

ASSOCIATED CONTENT

Supporting Information

The Supporting Information is available free of charge at https://pubs.acs.org/doi/10.1021/acs.est.4c01496.

The configuration of the MBfR system, compositions of the stock solutions (per liter of deionized H_2O), detailed sequencing and analysis processes of metagenomic, figures of XRD spectra, XPS spectra, and equivalent electron profile (PDF)

AUTHOR INFORMATION

Corresponding Author

Siqing Xia − *State Key Laboratory of Pollution Control and Resource Reuse, College of Environmental Science and Engineering, Tongji University, Shanghai 200092, China; Shanghai Institute of Pollution Control and Ecological Security, Shanghai 200092, China;* orcid.org/0000-0002-5613-2681; Email: siqingxia@gmail.com

Authors

Jingzhou Zhou − *State Key Laboratory of Pollution Control and Resource Reuse, College of Environmental Science and Engineering, Tongji University, Shanghai 200092, China; Shanghai Institute of Pollution Control and Ecological Security, Shanghai 200092, China*

Lin Yang − *State Key Laboratory of Pollution Control and Resource Reuse, College of Environmental Science and Engineering, Tongji University, Shanghai 200092, China;*

https://doi.org/10.1021/acs.est.4c01496
Environ. Sci. Technol. XXXX, XXX, XXX−XXX

Shanghai Institute of Pollution Control and Ecological Security, Shanghai 200092, China

Xiaodi Li − *State Key Laboratory of Pollution Control and Resource Reuse, College of Environmental Science and Engineering, Tongji University, Shanghai 200092, China; Shanghai Institute of Pollution Control and Ecological Security, Shanghai 200092, China*

Ben Dai − *State Key Laboratory of Pollution Control and Resource Reuse, College of Environmental Science and Engineering, Tongji University, Shanghai 200092, China; Shanghai Institute of Pollution Control and Ecological Security, Shanghai 200092, China*

Junxia He − *State Key Laboratory of Pollution Control and Resource Reuse, College of Environmental Science and Engineering, Tongji University, Shanghai 200092, China; Shanghai Institute of Pollution Control and Ecological Security, Shanghai 200092, China*

Chengyang Wu − *School of Environment and Architecture, University of Shanghai for Science and Technology, Shanghai 200093, China*

Si Pang − *Eco-Environmental Protection Research Institute, Shanghai Academy of Agricultural Science, Shanghai 201403, China*

Bruce E. Rittmann − *Biodesign Swette Center for Environmental Biotechnology, Arizona State University, Tempe, Arizona 85287-5701, United States;* orcid.org/0000-0002-3678-149X

Complete contact information is available at: https://pubs.acs.org/10.1021/acs.est.4c01496

Notes

The authors declare no competing financial interest.

■ ACKNOWLEDGMENTS

This work is supported by the National Key Project of Research and Development Plan of China (Grant No. 2021YFC3201300) and Shanghai Leading Talent Project (Grant No. 070).

■ REFERENCES

(1) Cao, F.; Jaunat, J.; Sturchio, N.; Cancès, B.; Morvan, X.; Devos, A.; Barbin, V.; Ollivier, P. Worldwide Occurrence and Origin of Perchlorate Ion in Waters: A Review. *Sci. Total Environ.* **2019**, *661*, 737−749.

(2) Wu, M.; Luo, J.-H.; Hu, S.; Yuan, Z.; Guo, J. Perchlorate Bio-Reduction in a Methane-Based Membrane Biofilm Reactor in the Presence and Absence of Oxygen. *Water Res.* **2019**, *157*, 572−578.

(3) Lai, C.-Y.; Wu, M.; Lu, X.; Wang, Y.; Yuan, Z.; Guo, J. Microbial Perchlorate Reduction Driven by Ethane and Propane. *Environ. Sci. Technol.* **2021**, *55* (3), 2006−2015.

(4) Zhang, B.; An, W.; Shi, Y.; Yang, M. Perchlorate Occurrence, Sub-Basin Contribution and Risk Hotspots for Drinking Water Sources in China Based on Industrial Agglomeration Method. *Environ. Int.* **2022**, *158*, No. 106995.

(5) WHO, G. Guidelines for Drinking-Water Quality. *World Health. Organ.* **2011**, *216*, 303−304.

(6) Lai, C.-Y.; Wu, M.; Wang, Y.; Zhang, J.; Li, J.; Liu, T.; Xia, J.; Yuan, Z.; Guo, J. Cross-Feeding Interactions in Short Chain Gaseous Alkane-Driven Perchlorate and Selenate Reduction. *Water Res.* **2021**, *200*, No. 117215.

(7) Butler, C. S.; Clauwaert, P.; Green, S. J.; Verstraete, W.; Nerenberg, R. Bioelectrochemical Perchlorate Reduction in a Microbial Fuel Cell. *Environ. Sci. Technol.* **2010**, *44* (12), 4685−4691.

(8) Zhao, H.-P.; Ontiveros-Valencia, A.; Tang, Y.; Kim, B.; Ilhan, Z. E.; Krajmalnik-Brown, R.; Rittmann, B. Using a Two-Stage Hydrogen-Based Membrane Biofilm Reactor (MBfR) to Achieve Complete Perchlorate Reduction in the Presence of Nitrate and Sulfate. *Environ. Sci. Technol.* **2013**, *47* (3), 1565−1572.

(9) Li, H.; Zhou, L.; Lin, H.; Zhang, W.; Xia, S. Nitrate Effects on Perchlorate Reduction in a H2/CO2-Based Biofilm. *Sci. Total Environ.* **2019**, *694*, 133564.

(10) Zhao, H.-P.; Van Ginkel, S.; Tang, Y.; Kang, D.-W.; Rittmann, B.; Krajmalnik-Brown, R. Interactions between Perchlorate and Nitrate Reductions in the Biofilm of a Hydrogen-Based Membrane Biofilm Reactor. *Environ. Sci. Technol.* **2011**, *45* (23), 10155−10162.

(11) Lv, P.-L.; Shi, L.-D.; Dong, Q.-Y.; Rittmann, B.; Zhao, H.-P. How Nitrate Affects Perchlorate Reduction in a Methane-Based Biofilm Batch Reactor. *Water Res.* **2020**, *171*, No. 115397.

(12) Dong, X.; Yu, K.; Jia, X.; Zhang, Y.; Peng, X. Perchlorate Reduction Kinetics and Genome-Resolved Metagenomics Identify Metabolic Interactions in Acclimated Saline Lake Perchlorate-Reducing Consortia. *Water Res.* **2022**, *227*, No. 119343.

(13) Streit, B. R.; Blanc, B.; Lukat-Rodgers, G. S.; Rodgers, K. R.; DuBois, J. L. How Active-Site Protonation State Influences the Reactivity and Ligation of the Heme in Chlorite Dismutase. *J. Am. Chem. Soc.* **2010**, *132* (16), 5711−5724.

(14) Chen, J.; Strous, M. Denitrification and Aerobic Respiration, Hybrid Electron Transport Chains and Co-Evolution. *Biochim. Biophys. Acta BBA - Bioenerg.* **2013**, *1827* (2), 136−144.

(15) Vignais, P. M.; Billoud, B. Occurrence, Classification, and Biological Function of Hydrogenases: An Overview. *Chem. Rev.* **2007**, *107* (10), 4206−4272.

(16) Luo, Y.-H.; Long, X.; Wang, B.; Zhou, C.; Tang, Y.; Krajmalnik-Brown, R.; Rittmann, B. E. A Synergistic Platform for Continuous Co-Removal of 1,1,1-Trichloroethane, Trichloroethene, and 1,4-Dioxane via Catalytic Dechlorination Followed by Biodegradation. *Environ. Sci. Technol.* **2021**, *55* (9), 6363−6372.

(17) Wu, C.; Zhou, L.; Zhou, Y.; Zhou, C.; Xia, S.; Rittmann, B. E. Dechlorination of 2,4-Dichlorophenol in a Hydrogen-Based Membrane Palladium-Film Reactor: Performance, Mechanisms, and Model Development. *Water Res.* **2021**, *188*, No. 116465.

(18) Luo, Y.-H.; Zhou, C.; Bi, Y.; Long, X.; Wang, B.; Tang, Y.; Krajmalnik-Brown, R.; Rittmann, B. E. Long-Term Continuous Co-Reduction of 1,1,1-Trichloroethane and Trichloroethene over Palladium Nanoparticles Spontaneously Deposited on H2-Transfer Membranes. *Environ. Sci. Technol.* **2021**, *55* (3), 2057−2066.

(19) Zhou, C.; Wang, Z.; Ontiveros-Valencia, A.; Long, M.; Lai, C.; Zhao, H.; Xia, S.; Rittmann, B. E. Coupling of Pd Nanoparticles and Denitrifying Biofilm Promotes H2-Based Nitrate Removal with Greater Selectivity towards N2. *Appl. Catal. B Environ.* **2017**, *206*, 461−470.

(20) Cheng, J.; Long, M.; Zhou, C.; Ilhan, Z.-E.; Calvo, D. C.; Rittmann, B. E. Long-Term Continuous Test of H2-Induced Denitrification Catalyzed by Palladium Nanoparticles in a Biofilm Matrix. *Environ. Sci. Technol.* **2023**, *57* (32), 11948−11957.

(21) Long, M.; Long, X.; Zheng, C.-W.; Luo, Y.-H.; Zhou, C.; Rittmann, B. E. Para-Chlorophenol (4-CP) Removal by a Palladium-Coated Biofilm: Coupling Catalytic Dechlorination and Microbial Mineralization via Denitrification. *Environ. Sci. Technol.* **2021**, *55* (9), 6309−6319.

(22) Zhou, J.; Wu, C.; Pang, S.; Yang, L.; Yao, M.; Li, X.; Xia, S.; Rittmann, B. E. Dissimilatory and Cytoplasmic Antimonate Reductions in a Hydrogen-Based Membrane Biofilm Reactor. *Environ. Sci. Technol.* **2022**, *56* (20), 14808−14816.

(23) Zhou, J.; Wu, C.; Pang, S.; Yang, L.; Yao, M.; Li, X.; Xia, S.; Rittmann, B. E. The Interplay of Sulfate and Nitrate Triggers Abiotic Reduction in a Hydrogen-Based Membrane Biofilm Reactor for Antimonate Removal. *Chem. Eng. J.* **2023**, *474*, No. 145798.

(24) Zhang, S.; Chen, Y.; Zhang, Z.; Ping, Q.; Li, Y. Co-Digestion of Sulfur-Rich Vegetable Waste with Waste Activated Sludge Enhanced Phosphorus Release and Hydrogenotrophic Methanogenesis. *Water Res.* **2023**, *242*, No. 120250.

(25) Wu, C.; Zhou, L.; Zhou, C.; Zhou, Y.; Xia, S.; Rittmann, B. E. Co-Removal of 2,4-Dichlorophenol and Nitrate Using a Palladized Biofilm: Denitrification-Promoted Microbial Mineralization Following Catalytic Dechlorination. *J. Hazard. Mater.* **2022**, *422*, No. 126916.
(26) Pang, S.; Rittmann, B. E.; Wu, C.; Yang, L.; Zhou, J.; Xia, S. Synergistic Inorganic Carbon and Denitrification Genes Contributed to Nitrite Accumulation in a Hydrogen-Based Membrane Biofilm Reactor. *Bioengineering* **2022**, *9* (5), 222.
(27) Rice, E. W.; Bridgewater, L.; Association, A. P. H. *Standard Methods for the Examination of Water and Wastewater*; American public health association: Washington, DC, 2012; Vol. *10*.
(28) Tang, Y.; Zhou, C.; Van Ginkel, S. W.; Ontiveros-Valencia, A.; Shin, J.; Rittmann, B. E. Hydrogen Permeability of the Hollow Fibers Used in H2-Based Membrane Biofilm Reactors. *J. Membr. Sci.* **2012**, *407*−*408*, 176−183.
(29) Lawson, C. E.; Wu, S.; Bhattacharjee, A. S.; Hamilton, J. J.; McMahon, K. D.; Goel, R.; Noguera, D. R. Metabolic Network Analysis Reveals Microbial Community Interactions in Anammox Granules. *Nat. Commun.* **2017**, *8* (1), 15416.
(30) Long, M.; Chen, Y.; Senftle, T. P.; Elias, W.; Heck, K.; Zhou, C.; Wong, M. S.; Rittmann, B. E. Method of H2 Transfer Is Vital for Catalytic Hydrodefluorination of Perfluorooctanoic Acid (PFOA). *Environ. Sci. Technol.* **2024**, *58* (2), 1390−1398.
(31) Wang, D. M.; Shah, S. I.; Chen, J. G.; Huang, C. P. Catalytic Reduction of Perchlorate by H2 Gas in Dilute Aqueous Solutions. *Sep. Purif. Technol.* **2008**, *60* (1), 14−21.
(32) Zhao, H.-P.; Ilhan, Z. E.; Ontiveros-Valencia, A.; Tang, Y.; Rittmann, B. E.; Krajmalnik-Brown, R. Effects of Multiple Electron Acceptors on Microbial Interactions in a Hydrogen-Based Biofilm. *Environ. Sci. Technol.* **2013**, *47* (13), 7396−7403.
(33) Coates, J. D.; Achenbach, L. A. Microbial Perchlorate Reduction: Rocket-Fuelled Metabolism. *Nat. Rev. Microbiol.* **2004**, *2* (7), 569−580.
(34) Ladhari, S.; Vu, N.-N.; Boisvert, C.; Saidi, A.; Nguyen-Tri, P. Recent Development of Polyhydroxyalkanoates (PHA)-Based Materials for Antibacterial Applications: A Review. *ACS Appl. Bio Mater.* **2023**, *6* (4), 1398−1430.
(35) Wang, H.-M.; Hu, G.-R.; Luo, W.-Y.; Li, F.-L. The Horizontal Gene Transfer of Perchlorate Reduction Genomic Island in Three Bacteria from an Ecological Niche. *Appl. Microbiol. Biotechnol.* **2024**, *108* (1), 22.
(36) Xie, T.; Yang, Q.; Winkler, M. K. H.; Wang, D.; Zhong, Y.; An, H.; Chen, F.; Yao, F.; Wang, X.; Wu, J.; Li, X. Perchlorate Bioreduction Linked to Methane Oxidation in a Membrane Biofilm Reactor: Performance and Microbial Community Structure. *J. Hazard. Mater.* **2018**, *357*, 244−252.
(37) Zhong, L.; Lai, C.-Y.; Shi, L.-D.; Wang, K.-D.; Dai, Y.-J.; Liu, Y.-W.; Ma, F.; Rittmann, B. E.; Zheng, P.; Zhao, H.-P. Nitrate Effects on Chromate Reduction in a Methane-Based Biofilm. *Water Res.* **2017**, *115*, 130−137.
(38) Chen, J.; Gu, M.; Zhou, Y.; Wan, D.; He, Q.; Shi, Y.; Liu, Y. Efficient Nitrate and Perchlorateremoval from Aqueous Solution via a Novel Electro-Dialysis Ion-Exchange Membrane Bioreactor. *Chem. Eng. J.* **2022**, *430*, No. 132952.
(39) Wan, D.; Wang, J.; Shi, Y.; Qu, D.; Zhang, J. Construction of Continuous-Flow Electrodialysis Ion-Exchange Membrane Bioreactor for Effective Removal of Nitrate and Perchlorate: Modelling and Impact Analysis of Environmental Variables. *Chem. Eng. J.* **2023**, *462*, No. 142144.
(40) Zhao, T.; Xie, B.; Yi, Y.; Zang, Y.; Liu, H. Two Polarity Reversal Modes Lead to Different Nitrate Reduction Pathways in Bioelectrochemical Systems. *Sci. Total Environ.* **2023**, *856*, No. 159185.
(41) Balk, M.; Mehboob, F.; van Gelder, A. H.; Rijpstra, W. I. C.; Damsté, J. S. S.; Stams, A. J. M. (Per)Chlorate Reduction by an Acetogenic Bacterium, Sporomusa Sp., Isolated from an Underground Gas Storage. *Appl. Microbiol. Biotechnol.* **2010**, *88* (2), 595−603.
(42) Liu, W.; Lian, J.; Guo, J.; Guo, Y.; Yue, L.; Niu, Y.; Duan, L. Perchlorate Bioreduction by Anaerobic Granular Sludge Immobilised with Fe-HA Complex: Performance, Extracellular Polymeric Substances and Microbial Community Structure. *J. Hazard. Mater.* **2020**, *398*, No. 122898.
(43) Bao, P.; Li, G.-X. Sulfur-Driven Iron Reduction Coupled to Anaerobic Ammonium Oxidation. *Environ. Sci. Technol.* **2017**, *51* (12), 6691−6698.
(44) Zheng, C.-W.; Zhou, C.; Luo, Y.-H.; Long, M.; Long, X.; Zhou, D.; Bi, Y.; Yang, S.; Rittmann, B. E. Coremoval of Energetics and Oxyanions via the In Situ Coupling of Catalytic and Enzymatic Destructions: A Solution to Ammunition Wastewater Treatment. *Environ. Sci. Technol.* **2023**, *57* (1), 666−673.

https://doi.org/10.1021/acs.est.4c01496
Environ. Sci. Technol. XXXX, XXX, XXX−XXX